Jet Energy Resolution and Scale Measurements for the ILD using Durham and MC Jet Clustering with $Z^* \to q\bar{q}$ Events

Niall McHugh, University of Glasgow, Scotland

September 5, 2018

Abstract

Jet energy resolution is a very important characteristic for any particle physics detector. For the ILD, the physics requirements demand that a never before achieved jet energy resolution (JER) of $\sim 3-4\%$ for 100 GeV jets must be achieved. Previously, JER for models of the ILD were calculated by taking the total reconstructed energy of each event and assuming that the reconstructed jet energies were exactly half of that, which is obviously an approximation. In this project, methods which instead calculated the resolution by reconstructing two distinct jets were investigated, namely Monte Carlo jet clustering and Durham jet clustering. Results showed that in every case the ILD model considered (ILD_l5_o1_v02) was able to achieve the required resolution and moreover that the total energy method gave similar values to the two jet clustering methods.

Contents

1 Introduction

The Standard Model (SM) is currently the best theoretical description of particle physics. It has successfully predicted the existence of a Higgs boson as the quantisation of the mass-giving Higgs field and the $W^{\pm}$ and Z bosons which mediate the weak force, along with correctly explaining all accepted high energy physics experimental results to date. It has however been known for some time to be incomplete. The most obvious discrepancy in the theory is its total omission of gravity; it also fails to include any candidate particles which could form the dark matter which astrophysicists have observed, or to explain why the universe has such an imbalance of matter and antimatter [1]. The International Linear Collider (ILC), which would be the most advanced e^+e^- collider to date, aims to provide a platform for continuing to probe such issues with the SM and thus further our theoretical understanding of the universe at the most fundamental level.

1.1 The International Linear Collider (ILC)

The ILC - as the name suggests - is a linear particle collider project. Using a linear collider as opposed to a circular collider avoids the issue of synchotron radiation, and makes upgrading the operating energy in the future a more straightforward procedure. It will measure 31km in length and be capable of operating at centre of mass energies of between 250 and 500 GeV initially, with a possible future upgrade to energies of up to 1 TeV [2]. An overview of the design is shown in Figure 1. This wide range of energies will allow for various studies at well suited energies [3]. The acceleration process will be accomplished using superconducting radio-frequency accelerator modules, the technology for which has already been extensively tested and then implemented at the FLASH and European XFEL sites at DESY [4]. At the collision point there will be one of two detectors: the International Large Detector (ILD) or the Silicon Detector (SiD), which will be periodically switched in and out of the collider every few weeks using a 'push-pull' system [5]. This report will focus on the ILD.

1.2 Particle Flow Reconstruction

Particle Flow is an approach to calorimetry which aims to improve detector resolution by reconstructing individual particles rather than just jets. This requires a highly granular calorimeter system for both electromagnetic and hadronic calorimeters, since energy deposits from different particles must be as well separated as possible. Ensuring this design means that the reconstruction algorithm can effectively associate the correct energy deposits to the correct particle. The result of using a Particle Flow Algorithm (PFA) is a collection of Particle Flow Objects (PFOs) at the end of the reconstruction, rather than just information about the jets in an event; these PFOs have various measured values such as energy, momentum, mass and can thus even be identified as specific particles. A PFA works by using a combination of hardware and software to For the ILC and thus

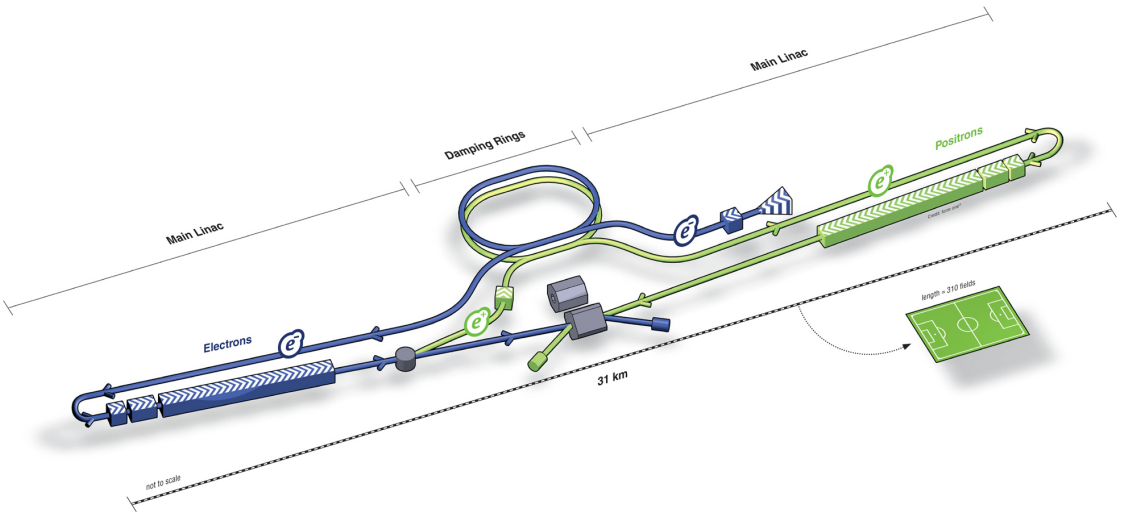

Figure 1: ILC Conceptual Diagram [6]

this report, the Particle Flow algorithm which is used is the PandoraPFA algorithm [7].

By using complex pattern recognition algorithms which assign specific sub-detector measurements to different reconstructed objects, PandoraPFA is able to reconstruct such a set of PFOs for analysis. Then, for each particle the energy measurement can be taken from only the most accurate detector subsystem in which it can be detected. For example, the energy of charged particles can be taken from the TPC rather than the calorimeters. Through this the overall resolution of the detector is improved, since the TPC has a much better energy resolution than the calorimeters. In this way, it is only necessary to take the less accurate calorimeter measurements for uncharged particles, which make up around 38% of the long-lived particles in jets resulting from e^+e^-collisions [8].

Attempts have been made to use a similar method in the past, namely using the 'energy flow' approach. While this was successful in improving jet energy resolution at ALEPH and other LEP experiments [9], the lack of calorimeter granularity in such detectors meant that the effectiveness of this method was in those cases limited, as individual particle reconstruction was not fully possible.

1.3 The International Large Detector (ILD)

The ILD aims to be the first high energy physics detector capable of allowing the particle flow approach to reconstruction to be truly implemented. The main difference between the ILD and previous detectors at other experiments will be the highly segmented nature of its calorimeters, which as stated in Section 1.2 is crucial for the implementation of

Particle Flow. The particle flow approach allows for much better jet energy resolution than has previously been possible with experiments at facilities such as LHC or LEP at CERN. Indeed, in order to satisfy the physics requirements of the ILD, a jet energy resolution of ∼3-4% for jets of 100 GeV is necessary [10]; this will allow the decays of the W and Z bosons to be cleanly separated.

The ILD will consist of several sub-detectors. Firstly, there will be a vertex detector, surrounded by a silicon tracker and a TPC. Then, there will be several layers of highly segmented electromagnetic and hadronic calorimeter tiles. This will be surrounded by a large superconducting coil producing a 3.5T axial magnetic field, which is further encased in a yoke which functions as a muon detector. Finally, there are also separate calorimeters in the forward regions so that the detector will provide the largest possible angular coverage for every event. An image displaying this design is shown in Figure 2.

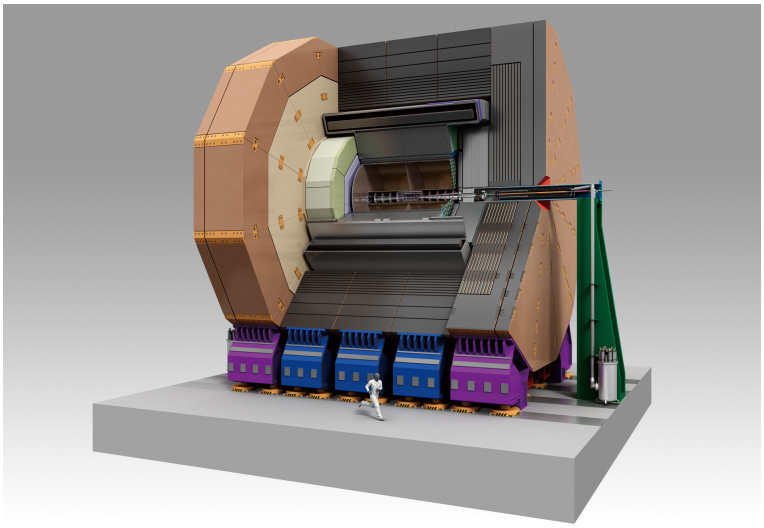

Figure 2: ILD Generated Image [11]

1.3.1 Jet Energy Resolution and Scale

The way in which detector performance is typically parameterised is by calculating the jet energy resolution and scale. The jet energy resolution is essentially a measure of the detector's ability to resolve the difference in energy between two jets of similar total energy. This can be measured by simulating numerous di-jet events at a known energy and calculating the resolution from the resulting spectrum of 'measured' energies. This will be discussed in more detail in Section 2.

The jet energy scale is a parameterisation of how accurately the detector measures the actual energy values. This can be shown on a plot of reconstructed jet energy against

simulated (true) jet energy which should agree with the line $y = x$ for a correctly calibrated detector and working clustering algorithm.

2 Methods

For the work in this report, the *Marlin* framework [12], using code written in *C++*, was used to manipulate files of the *LCIO* [13] data format. This was provided within the *iLCSoft* framework [14], of which version v02-00-01 was used. The ILD detector model ILD_l5_o1_v02 was used for all simulations. A separate piece of *C++* code was used to calculate the resolution at each energy for each method and to produce all *ROOT* [15] plots for jet energy resolution and scale which are shown. Further plots were created directly using *ROOT* macros to analyse data output from the *Marlin* processors. For performing Durham jet clustering, the *FastJet* plugin was used [16].

2.1 Monte Carlo (MC) Simulation Samples

As stated in Section 1.3.1, to measure the jet energy resolution of a detector it is necessary to simulate many events within a model of the detector. For this report, the simulated events consisted of an initial e^+e^- collision at chosen $\sqrt{s}$ forming a fictional, stationary Z boson with $m_Z = \sqrt{s}$. Then, a decay to a $q\bar{q}$ pair was forced, with momenta clearly opposite to each other in order to satisfy conservation of momentum. In the simulation the quarks then further decay into a parton shower, undergo a hadronisation process and in some cases further decays until they form the particles which actually interact with the detector. The $q\bar{q}$ pair used was always up, down or strange so that the number of neutrinos in each event was kept as low as possible; this is because neutrinos are not measured by the detector. While the initial quarks energies must each be exactly one half of the centre of mass energy, through subsequent interactions in the parton shower stage this balance can be altered.

2.2 Measurement of Jet Energy Resolution and Scale

In this report three different approaches to calculating the jet energy resolution were utilised, by performing some calculations on a data set filled by taking reconstructed energy across many events from: the total reconstructed energy, Monte Carlo clustered jets and Durham clustered jets. For both jet clustering methods, the calculations were identical and for the total energy method a slight correction was applied, described in Section 2.3. Firstly, a histogram was filled with relevant the relevant energies measured in each case. Then, the resolution was calculated from this histogram by taking the ratio of:

$$\text{Res.} = \frac{\text{rms}_{90}}{\text{mean}_{90}} \tag{1}$$

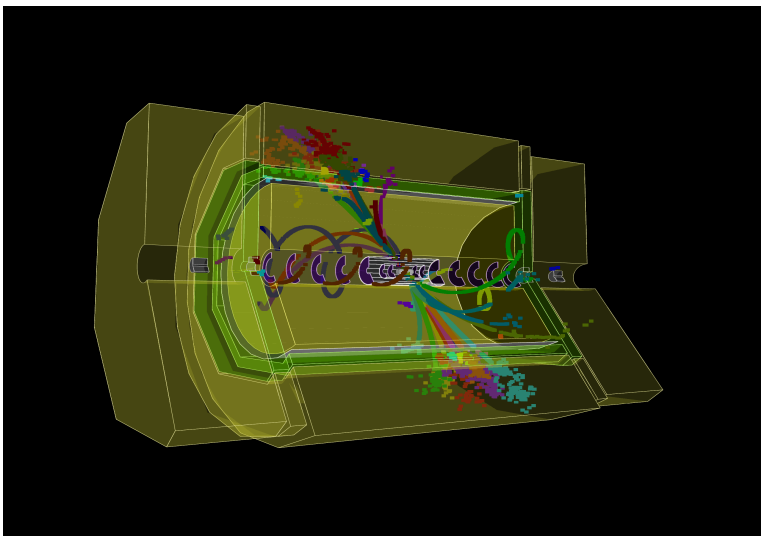

Figure 3: Example PFOs from 240 GeV $e^+e^- \to Z^* \to q\bar{q}$ event, taken from *C Event Display* (CED) screenshot [17]

Here rms_{90} and mean_{90} are the rms and mean of a modified energy distribution containing only the central 90% of events [18]. The obtained values for resolution were then plotted against half the centre of mass energy to give a plot of jet energy resolution as a function of jet energy.

The value for reconstructed jet energy was taken to be simply as mean_{90} or $\text{mean}_{90}/2$ for the cases of jet clustering and total energy respectively, which was then be plotted against the true jet energy to form the jet energy scale plot.

In every case, 5000 events were simulated. This number was however reduced by applying a cut to include only events where the difference in jet energies at the MC level was below a given threshold. This was to ensure that the approximations made by the total energy method - given in Section 2.3 - were valid in all events considered for the purposes of calculating resolution. This is described in more detail in Section 3.1.

2.3 Total Energy Method

The first method used to calculate the resolution considered only the total reconstructed energy from all PFOs. These energies were summed and filled into a histogram. Then, the approximation $E_{jet} = E_{jet\ 1} \approx E_{jet\ 2} \implies E_{jet} \approx E_{tot}/2$ was taken. By extending this assumption to the errors for each jet energy being approximately the same and adding in quadrature we find that $\sigma_{E_{jet}} = \sigma_{E_{jet\ 1}} \approx \sigma_{E_{jet\ 2}} \implies \sigma_{E_{jet}} \approx \sigma_{E_{tot}}/\sqrt{2}$. This finally gives the jet energy resolution as [19]:

$$\frac{\sigma_{E_{jet}}}{E_{jet}} \approx \sqrt{2}\frac{\sigma_{E_{tot}}}{E_{tot}} \tag{2}$$

Here the values measured - as described in Section 2.2 - from the distribution were the rms_{90} and mean_{90} for the total energy histogram which then gave the scale and allowed the resolution in terms of jet energy to be calculated via Equation 2. This method was implemented using code which was already available in the *ILDPerformance* library for *iLCSoft* [20].

2.4 Monte Carlo Jet Clustering

The second method used involved clustering all the reconstructed PFOs into two jets using Monte Carlo information from the simulation, giving two separate jet energies per event. This was achieved by first collecting a list of all MC particles from the simulation which resulted from the hadronisation process, as well as any photons produced previously. The momentum of the initial quarks was then used to divide a coordinate system, with origin at the collision point, into two hemispheres representing where each jet should lie. Implicit in this step is the assumption that at the energies considered the two jets are, just after hadronisation, collinear enough in opposite directions to ensure is no possibility of overlap between jets. Then, the daughters of the particles in each jet were iterated over recursively until every MC particle present in the simulation had been assigned to a jet. The final step was then to use the reconstructed particle to MC particle links provided by *Marlin* in order to split the PFOs into two jets to obtain the energy of each jet. Then, analysis was performed as described in Section 2.2.

2.5 Durham Jet Clustering

The final method investigated was jet clustering using the Durham (e^+e^- k_t) algorithm, a method which could actually be used to reconstruct jets from real event data. The Durham algorithm is performed by first computing a 'distance' between all pairs of reconstructed particles, defined by d_{ij} for particles i and j [21]:

$$d_{ij} = 2\text{min}(E_i^2, E_j^2)(1 - \text{cos}\theta_{ij}) \tag{3}$$

Here $E_{i(j)}$ is the energy of particle $i(j)$ and θ_{ij} is the angle between the momenta of the two particles. The algorithm then iteratively combines the 'closest' particles into one object, and continues doing so until a terminating condition occurs. Here, the condition was when all particles had been combined into two jets, since all events considered were di-jet. For combining particles, simple 4-vector addition was used. After performing this process for each event the analysis given in Section 2.2 was again performed on a distribution of all jet energies. All jet clustering performed in this way was completed using the *FastJet* software package, included in *iLCSoft* [22, 23].

3 Results

3.1 Initial Results

The total energy method was expected to perform the best because it does not rely at all on clustering algorithms, but only on the difference between the true energy in an event and the reconstructed energy. It was then expected that MC clustering should give the next best results; while it does rely on the clustering approach, it has full access to all simulation data and so the only possible sources of clustering errors occur from any confusion in the stage linking PFOs to MC particles. Finally, Durham clustering was expected to give worse resolution than the other two methods because it relied on jet clustering using only the final reconstructed particles, so was expected to make more clustering mistakes than the MC method.

Initial plots using a preliminary 1000 simulated events at each energy showed that while the total energy method did give the lowest resolution values by a margin of approximately 2%, MC and Durham clustering performed the same to within a margin of error. It was soon realised however that these results were incorrect, as in the simulated events the individual jet energies were not always exactly equal. A distribution of MC jet energy for these 1000 events at 200 GeV is shown in Figure 4 to illustrate this. The symmetry of the histogram arises from the energies of the jets always summing to $\sqrt{s}$.

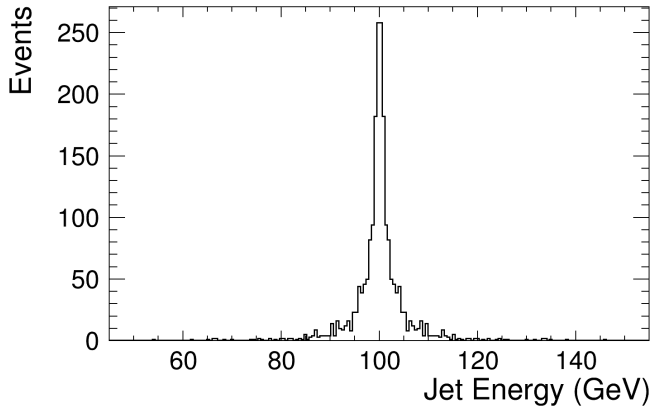

Figure 4: Distribution of MC jet energies for 1000 events at $\sqrt{s} = 200$ GeV

The distributions which were used to calculate the resolution for the total energy had width only due to the difference between the total true energy of the particles interacting with the detector and the total measured energies. For both clustering methods the distributions had some width from similar errors, but also an additional spread due to this asymmetry between the true energy of the jets within the simulation which were being reconstructed. This essentially meant that the results calculated for the MC and Durham methods were not actually calculating the resolution only at the correct energy

value, but over a range of nearby energies. Thus, it is clear that some selection of events must be applied in order to give a fair comparison between the different methods. Two different solutions to this problem were investigated:

- Applying a cut to eliminate events where the true jet energies were too asymmetric
- Splitting up all reconstructed jets into several 'bands' based on MC level jet energy to subsequently calculate several resolution data points for each $\sqrt{s}$

3.1.1 Cuts on Asymmetric Events

The first method attempted was cutting events which were too asymmetric within the simulation from the final analysis process. Table 1 shows the number of events from the initial 5000 remaining at each energy after several different cuts were applied. Figure 5 also shows how the distribution shown in Figure 4 changes with these cuts. Finally, Figure 6 shows how the distributions of reconstructed jet energies from the MC clustering approach change with these cuts. The initial idea behind this method was to select only events where the approximations made by the total energy method were valid.

Whilst applying this cut does somewhat improve the percentage of events where the approximations are met, it still does not completely satisfy the aim of allowing for a fair comparison. This is because although there is a correlation between reconstructed jet energy and MC jet energy, it is not the case that simulating jets of equal energy will result in two reconstructed jets which are also of equal energy. In addition to this, it would not make sense to apply a cut at the reconstructed jet energy level since the reconstructed jet energy is dependent on the jet clustering method used. Thus, it was concluded that there is no quantitative way to truly compare the total energy method with jet clustering approaches; they must simply be taken as two different approaches to parameterising detector performance.

Table 1: Number of remaining events after MC jet energy difference cuts

Energy (GeV)	$E_{mc\ diff} \leq 1\%\sqrt{s}$	$E_{mc\ diff} \leq 3\%\sqrt{s}$	$E_{mc\ diff} \leq 10\%\sqrt{s}$
40	986	2475	4463
91	1499	3176	4358
200	2047	3437	4585
350	2244	3491	4596
500	2353	3614	4608

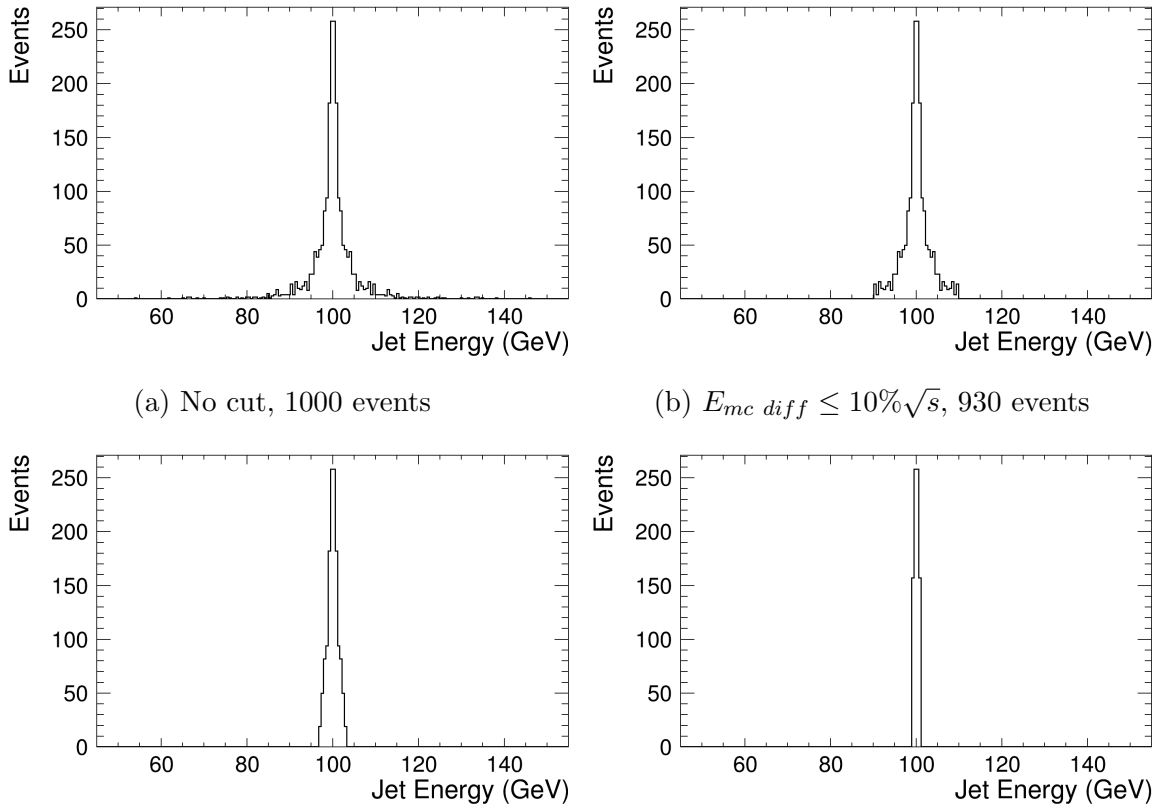

(a) No cut, 1000 events

(b) $E_{mc\ diff} \leq 10\%\sqrt{s}$, 930 events

(c) $E_{mc\ diff} \leq 3\%\sqrt{s}$, 685 events

(d) $E_{mc\ diff} \leq 1\%\sqrt{s}$, 415 events

Figure 5: Distribution of MC jet energies for 1000 events at $\sqrt{s} = 200$ GeV with different asymmetry cuts

3.1.2 MC 'Banding' Approach

Whilst the process of eliminating certain events does succeed in allowing a fair comparison between different methods of measuring resolution, it does have the downside that as many as $\sim 80\%$ of events can go unused. Thus, the method of dividing the reconstructed energies into several groups based on their MC energies and calculating several points was proposed to make use of as many events as possible. In practice, it is impossible to make use of every single event since for the furthest MC jet energies from the mean there are so few events that the large statistical errors at those MC energies render the resolution values which are calculated meaningless.

This initially looked to produce promising results, however it was quickly realised that there is a flaw in this method. Dividing the distribution shown in Figure 4 into bands necessarily creates several distributions skewed towards the centre of the entire distribution. Thus, the reconstructed energy distributions are also skewed in the same direction; the methods used here to calculate rms_{90} and mean_{90} are not valid since they assume

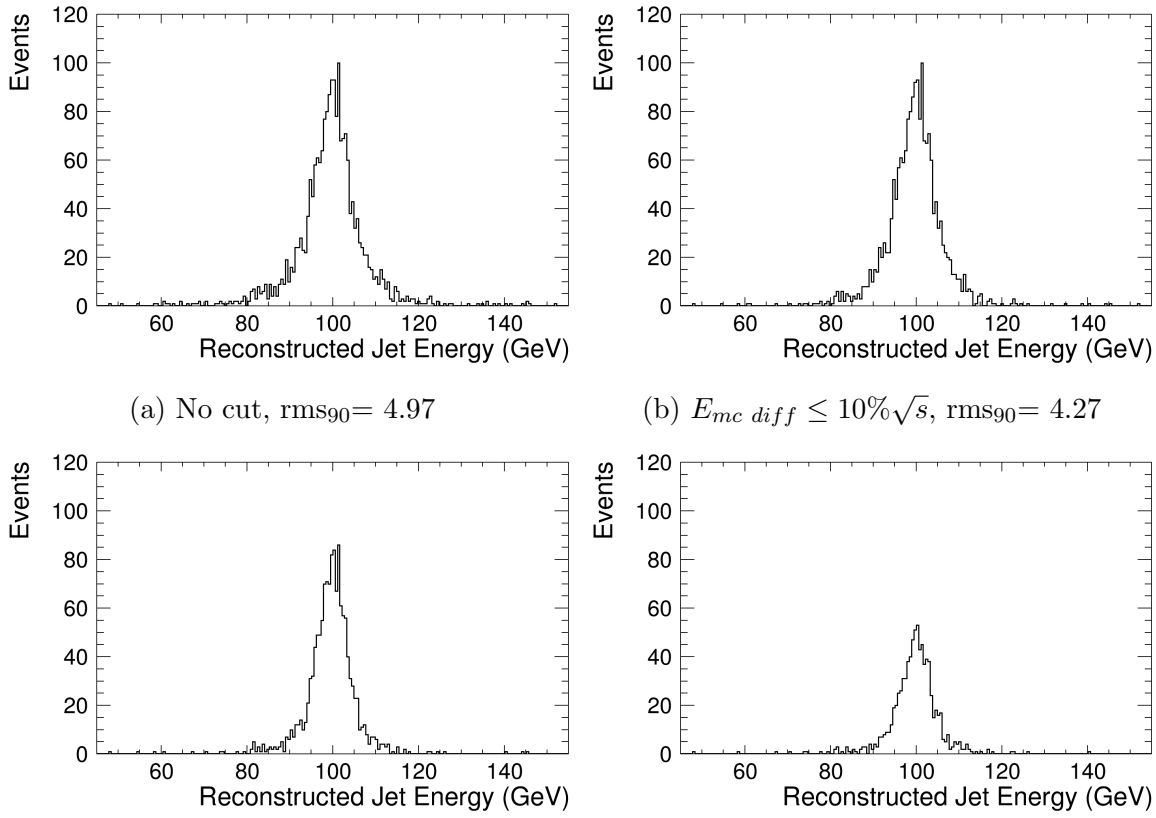

(a) No cut, rms_{90}= 4.97

(b) $E_{mc\ diff} \leq 10\%\sqrt{s}$, rms_{90}= 4.27

(c) $E_{mc\ diff} \leq 3\%\sqrt{s}$, rms_{90}= 3.45

(d) $E_{mc\ diff} \leq 1\%\sqrt{s}$, rms_{90}= 3.44

Figure 6: Distribution of reconstructed MC clustering jet energies for 1000 events at $\sqrt{s} = 200$ GeV with different asymmetry cuts

an at least almost symmetrical distribution. While it would be possible to use different statistical methods and obtain a correct result, this was not attempted due to time constraints and the availability of another functioning method, namely applying MC level cuts.

3.2 Jet Energy Resolution (JER) Results

As stated in Section 3.1.1 it was concluded that there is no way to obtain a true comparison between the total energy method and jet clustering methods of calculating jet energy resolution. Thus, the results are given separately here, with only a comparison between the jet clustering methods plotted. It was decided that the best compromise between retaining events and ensuring accuracy of the true jet energy was to apply a cut of $E_{mc\ diff} \leq 1\%\sqrt{s}$ when calculating resolution using jet clustering.

3.2.1 Total Energy Method

Figure 7 shows the jet energy resolution as calculated using the total energy method for the barrel region of the detector and also against $|\cos\theta|$ of the initial quarks - with $|\cos\theta| = 1$ being directly along the beam pipe and $|\cos\theta| = 0$ straight into the barrel. More plots showing jet energy resolution for the whole detector can be found in Appendix A.

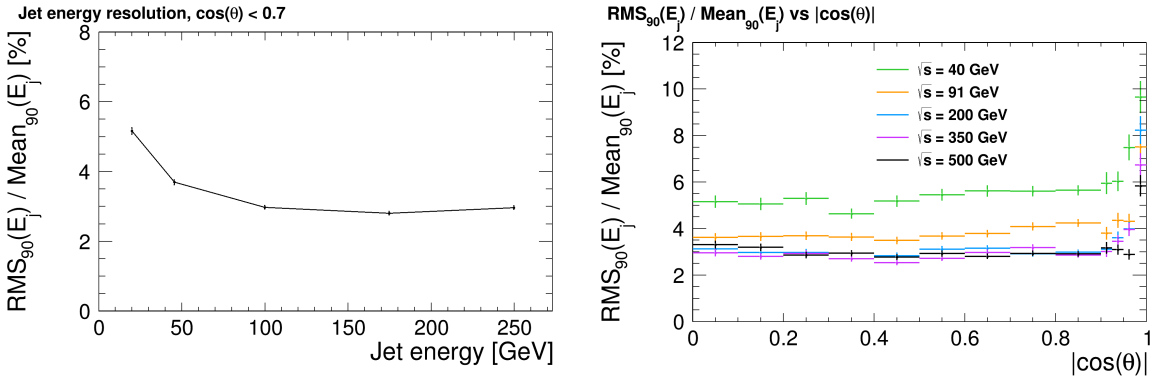

(a) JER vs. jet energy, barrel region

(b) JER vs. $|\cos\theta|$

Figure 7: Jet energy resolution for total energy method

3.2.2 Jet Clustering Methods

Figure 8 shows how the JER varies with jet angle for each jet clustering method. Figure 9 shows the JER for both jet clustering methods against jet energy in the barrel region of the detector. More plots showing JER for the whole detector using both methods, and also how this changes as different MC level cuts are applied can be found in Appendix B.

3.3 Jet Energy Scale (JES) Results

Figure 10 shows the jet energy scale results for each method. In each case, $y = x$ is also plotted in red for reference.

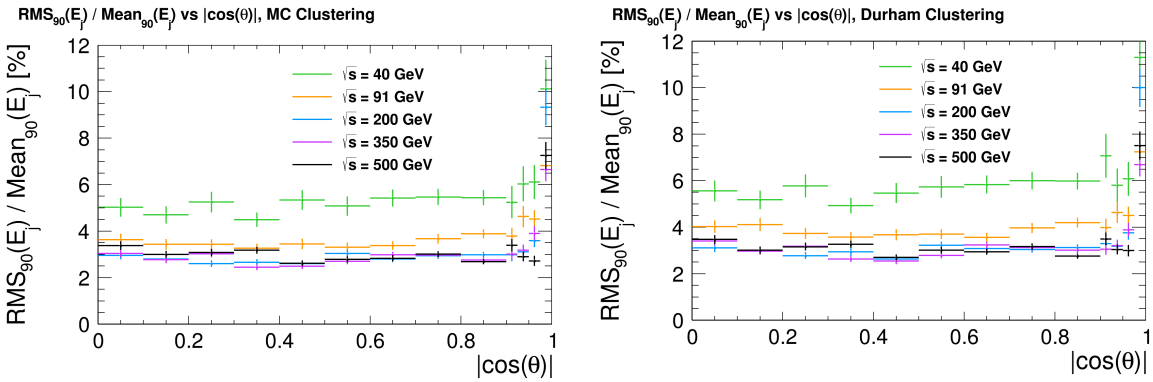

(a) MC clustering (b) Durham clustering

Figure 8: Jet energy resolution against $|\cos\theta|$ for jet clustering methods

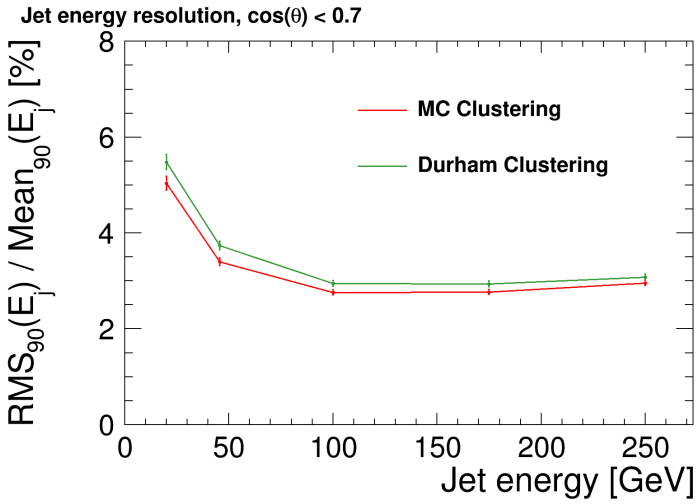

Figure 9: Jet energy resolution against jet energy for jet clustering methods, barrel region

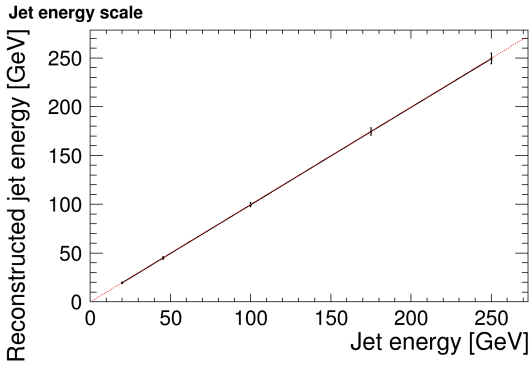

(a) Total energy method

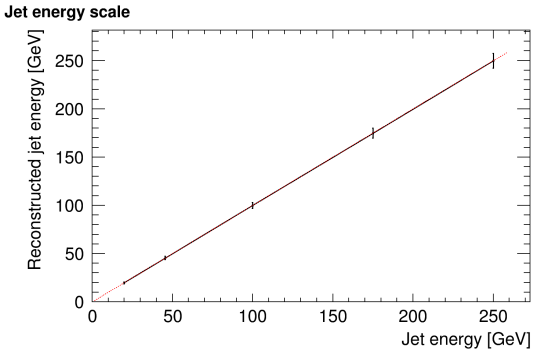

(b) MC Clustering method

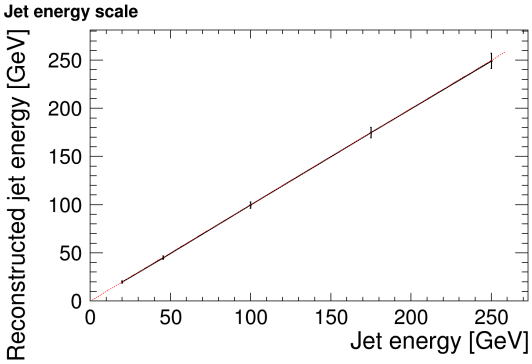

(c) Durham Clustering method

Figure 10: Jet energy scale plots for all three methods with $y = x$ line

4 Conclusion

The initial aim of this project was to investigate jet clustering methods, and compare these to the already implemented total energy method in order to see what effect its approximation had on the calculated jet energy resolution of the ILD detector. As stated in Section 3.1.1 however, it was found that there was no fair way to select events where this approximation was valid and thus a fair comparison is not possible. It should however be noted by looking at the barrel region resolution plots for each method that one conclusion which can be drawn is that the effect of applying the total energy approximation is actually very small in the case of these uds events. As well as this, for every method the requirement upon the JER of reaching $\sim 3-4\%$ at 100 GeV is achieved.

In addition, using MC clustering provides better resolution than Durham clustering. This was to be expected since MC clustering has full access to the simulation of each event and should thus make very few, if any, clustering mistakes. It should however be noted that at high energies there appears to be less distinction between the methods; this is most likely because at such high energies each jet is collinear enough and well enough separated from the other that there is very little confusion as to which jet each particle belongs. MC clustering is here interpreted as the best possible jet energy resolution for a specific detector model and reconstruction configuration; Durham clustering is closer to the jet energy resolution expected for real data, however it should be remembered that this case of two back-to-back jets is the simplest possible case for a jet clustering algorithm to process.

From the jet energy scale plots, everything is indeed linear and in agreement with the line $y = x$ as expected. This means that the parameters within the detector model and reconstruction algorithms are correctly calibrated.

5 Acknowledgements

Firstly, I would like to thank my supervisor, Remi, for guiding me through this project, providing assistance whenever I was unsure of something and having to deal with my constant bombardment of emails with new plots or results every day (even on holiday). I would like to thank Jakob and Eldwan, who were also especially patient when I bothered them with lots of beginner's questions whenever I wasn't able to get hold of Remi. I would also like to thank all the members of the FLC group here at DESY who welcomed us into their department as colleagues and helped make our time here thoroughly enjoyable.

Finally, I would like to thank Olaf and everyone else who was involved with coordinating the summer student program, organising events for us and lecturing us on so many interesting aspects of high energy physics.

References

[1] CERN, "The Standard Model", Accessed: 03/09/18, URL: https://home.cern/about/physics/standard-model

[2] C. Adolphsen (ed.) *et al.*, "The International Linear Collider Technical Design Report, Volume 3: Accelerator, Part II: Accelerator Baseline Design", arXiv:1306.6328 (2013)

[3] H. Baer (ed.) *et al.*, "The International Linear Collider Technical Design Report, Volume 2: Physics", arXiv:1306.6352 (2013)

[4] C. Adolphsen (ed.) *et al.*, "The International Linear Collider Technical Design Report, Volume 3: Accelerator, Part I: R&D in the Technical Design Phase", arXiv:1306.6353 (2013)

[5] T. Behnke (ed.) *et al.*, "The International Linear Collider Technical Design Report, Volume 4: Detectors", arXiv:1306.6329 (2013)

[6] ILC GDE, "ILC Conceptual Design", Accessed: 21/08/18, URL: http://www.linearcollider.org/images/pid/1000890/gallery/11_ILC_schematic_image%28E%29.jpg

[7] J. S. Marshall and M. A. Thomson, "The Pandora Software Development Kit for Particle Flow Calorimetry", *J. Phys.: Conf. Ser.*, **396**, 022034 (2012)

[8] M. A. Thomson, "Particle Flow Calorimetry and the PandoraPFA Algorithm", arXiv:0907.3577 (2009)

[9] ALEPH Collaboration, D. Buskulic et al., Nucl. Instr. and Meth. **A360** 481 (1995)

[10] ILD Concept Group, "ILD Letter of Intent", arXiv:1006.3396 (2010)

[11] R. Hori/KEK, "ILC International Large Detector (ILD)", Accessed: 21/08/18, URL: http://www.linearcollider.org/images/pid/1000890/gallery/15_ILC_ILD.jpg

[12] F. Gaede, Nucl. Instr. and Meth. **A559** 177 (2006)

[13] F. Gaede, T. Behnke, N. Graf, and T. Johnson, "LCIO: A persistency framework for linear collider simulation studies", Proceedings of CHEP 03, La Jolla, California, arXiv:physics/0306114 (2003)

[14] iLCSoft Software Package, Accessed: 22/08/18, URL: https://github.com/iLCSoft

[15] R. Brun and F. Rademakers, "ROOT - An Object Oriented Data Analysis Framework", Proceedings AIHENP'96 Workshop, Lausanne, Nucl. Inst. and Meth. **A389** 81-86 (1996). See also root.cern.ch/.

[16] M. Cacciari, G.P. Salam and G. Soyez, Eur.Phys.J. **C72** 1896, arXiv:1111.6097, (2012)

[17] H. Hölbe, "C Event Display (CED) User Manual", Accessed: 23/08/18, URL: `http://ilcsoft.desy.de/CED/current/doc/manual.pdf` (2012)

[18] J. S. Marshall, A. Munnich and M. A. Thomson, "Performance of Particle Flow Calorimetry at CLIC", arXiv:1209.4039 (2012)

[19] J. S. Marshall and M. A. Thomson, "Pandora Particle Flow Algorithm", arXiv:1308.4537 (2013)

[20] ILDPerformance Software Package, Accessed: 22/08/18, URL: `https://github.com/iLCSoft/ILDPerformance`

[21] M. Cacciari, G. P. Salam and G. Soyez, "FastJet User Manual", arXiv:1111.6097 (2011)

[22] M. Cacciari, G. P. Salam and G. Soyez, FastJet Software Package, Accessed: 22/08/18, URL: `http://www.fastjet.fr/`

[23] Marlin interface for FastJet, Accessed: 22/08/18, URL: `https://github.com/iLCSoft/MarlinFastJet`

Appendix A

Shown here are further jet energy resolution plots for the total energy method.

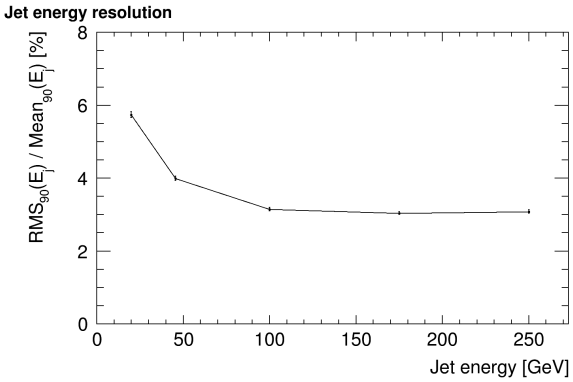

Jet energy resolution for the entire detector with 5000 events, total energy method

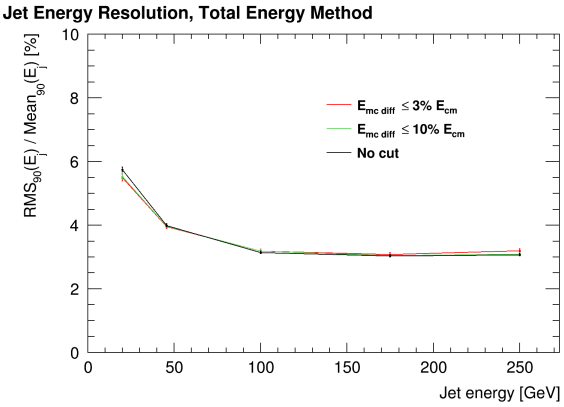

Jet energy resolution for the entire detector with 5000 events and various MC jet energy difference cuts, total energy method

Appendix B

Shown here are further jet energy resolution plots for the jet clustering methods. Note how for these methods the jet energy resolution changes significantly as the cut is altered, whereas it does not change for the total energy method. This is as discussed in Section 3.1.

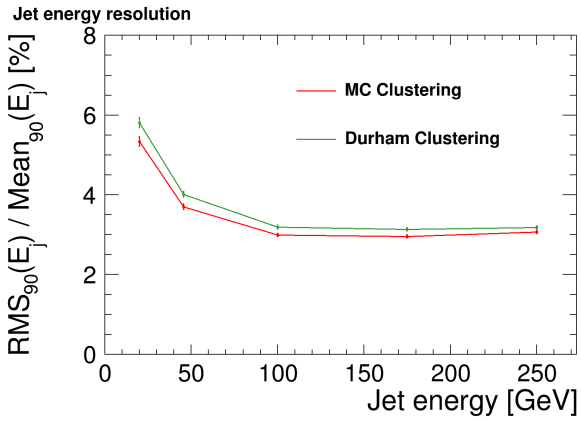

Jet energy resolution for the entire detector with 5000 events before $E_{MC\ diff} \leq 1\%\sqrt{s}$ cut, jet clustering methods

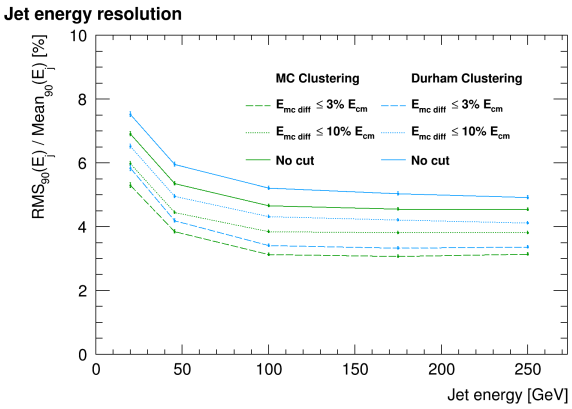

Jet energy resolution for the entire detector with 5000 events and various MC jet energy difference cuts, jet clustering methods

Appendix C

Shown here is the result of a brief study into how altering the bin width affected the calculated values for jet energy resolution. The calculated values change because the algorithm computing the resolution (from ILDPerformance) takes all counts in each bin as occurring at the bin center, not the value they had before binning. These results were obtained using just 1000 events with no cuts to avoid MC level asymmetry, but the principle holds for larger numbers of events. From these results it was decided that bin width/jet energy should always be much smaller than 10^{-2}.

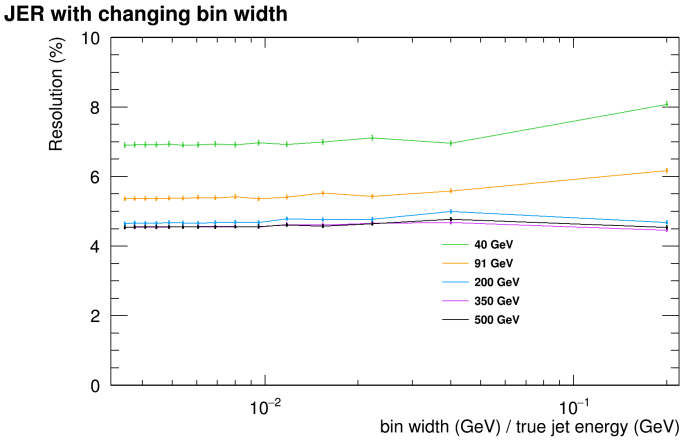

JER for various bin widths with varying $\sqrt{s}$

Appendix D

Shown here is a plot of jet energy resolution for the whole detector using MC clustering, with and without adding the energy of all neutrinos in each jet to the final reconstructed jet energy. From this it was concluded that for the uds events considered, the effect of neutrinos on the final energies was negligible.

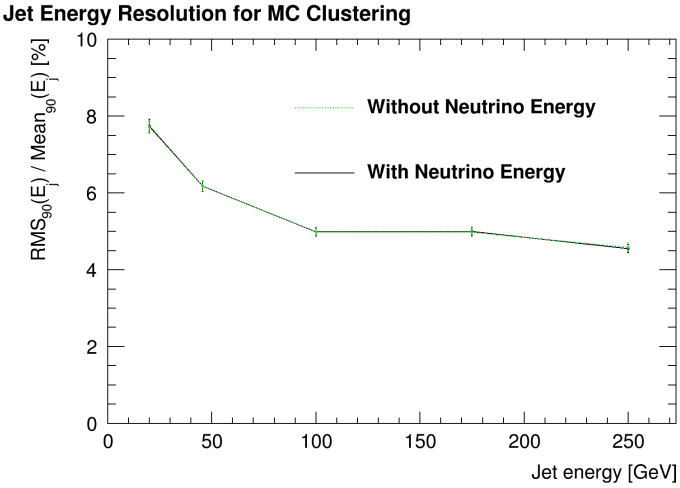

JER plot with and without adding neutrino energy, MC clustering